UVX 2008 (2009) 45–50

DOI: 10.1051/uvx/2009008

High harmonics generation: Spatial characterisation and applications

J. Gautier[1], P. Zeitoun[1], A.S. Morlens[1], S. Sebban[1], C. Valentin[1], E. Papalazarou[1], J.P. Goddet[1], G. Lambert[1], T. Marchenko[1] and M. Fajardo[2]

[1] *Laboratoire d'Optique Applique ENSTA Palaiseau, France*
[2] *Insituto Superior Tecnico, Av. Pais Rovisco, Lisbon, Portugal*

Abstract. We present a full optimization of the high harmonics wave-front thanks to the use of a soft x-ray Hartmann sensor. The sensor was calibrated using high harmonics source with a $\lambda/50$ accuracy. We observed relatively good high harmonics wave-front, two times the diffraction-limit, with astigmatism as the dominant aberration for any interaction parameters.The influence of high harmonic generation parameters was also studied in particularly the influence of the infra-red wave-front. This wave front quality allows applications by focalization of this beam. We present experiment we performed on damage target and holography.

1. INTRODUCTION

The past decade has witnessed the emergence of high brightness table top Extreme Ultra Violet (EUV) sources as high harmonics generation (HHG), or plasma based soft x-ray laser (SXRL). This development is motivated by the large field of applications as microscopy[1], phase contrast imaging[2] and holography[3,4]. These sources have demonstrated a high brightness[5] and high degree spatial coherence[7]. However, for experiments concerning phase imagining or tight focusing, EUV beam must have high optical quality, and more precisely a diffracted limited wave front. The Marechal's criterion[8] stands that a beam is diffraction-limited at a given wavelength, λ, when the root-mean-square (rms) wave front aberration is lower than $\lambda/14$. EUV wave-front can be reconstructed by several techniques[8,9]. In these experiments we have used the so-called Hartmann techniques. In this paper, we first present the principle and the calibration of the Hartman sensor. This sensor is used to characterize high harmonics wave front and to study the influence of high harmonics generation. In the second part two application of this low abberation wavefront are presented. The first one is the study of the damage of target induced by XUV pulse. The second one is holography experiments.

2. WAVE FRONT MEASUREMENT

2.1. Hatmann calibration

The Hartmann wave front sensor is based on mapping the wave vectors at numerous locations across the wave-front. The incoming beam is divided by a hole array into a large number of sub-rays monitored in intensity and position by a CCD camera. The positions of the individual spot centroids are determined and compared with a reference position. The soft x-ray Hartmann sensor was made of a 100 μm thick, nickel plate placed at about 20 cm in front of the CCD camera. The plate is constituted of 51 $\times$ 51 square holes, 80 μm in size each, and separated by 380 μm over a 15×15 mm^2 area. The projected spot pattern was recorded on a cooled back illuminated CCD having 2048×2048 pixels operating at $-40\,^{\circ}$C. The pixel size was $13.5 \times 13.5\ \mu$m^2. For calibration purpose, we generated the reference spherical wave front by diffracting the EUV beam onto a 10 μm pinhole placed 3.3 m away from the Hartman sensor. The XUV beam was constituted of four consecutive high harmonics ($\lambda = 28$ nm to $\lambda = 41$ nm) dominated

by the 25th harmonics ($\lambda = 32$ nm). The experiment set-up is shown on Fig. 1. The high harmonics are generated by focusing a Ti:Sa femtosecond laser (1 kHz, 800 nm, 6 mJ, 40 fs) with a f = 1 m lens in an argon gas cell. The parameters of the gas cell (length and gas pressure), of the infrared beam (energy and pulse duration) and of the focusing lens (position) were initially adjusted such as to optimize the HHG flux at 32 nm. A 300 nm thin aluminum filter has been used to filter out the infrared beam. Notice that the pinhole was placed at about 1 m away from the HHG source, where the beam is about 1 mm in diameter, and no soft x-ray focusing optic was used. With this pinhole, the first Airy disk's diameter is 25.7 mm on the Hartmann plate. The diffracted-beam being much larger than the plate ensured to use a high-quality wave front for calibration. The filter diameter then reduced the illuminated CCD area to a disk of 11.2 mm in diameter, therefore the calibration of the sensor was performed over 32 × 32 sub-pupils centered on the CCD chip. The acquisition time was about 20 mn. The residual absolute wave front has a value of 0.02 λ EUV rms and 0.08 λEUV peak-to-Valley (PV). Accuracy measurement was performed by translating the 10 μm pinhole by 110 μm, transversally to the beam propagation axis. Good agreement was observed between the translation calculated with the Hartmann wave front sensor software and the real one given by a motorized 0.1-μm-accurate translation stage. The absolute wave front was 0.04λ rms and 0.2λ PV. We experimentally measured the sensor accuracy to be λ/50 root-mean-square (rms) with $\lambda = 32$ nm.

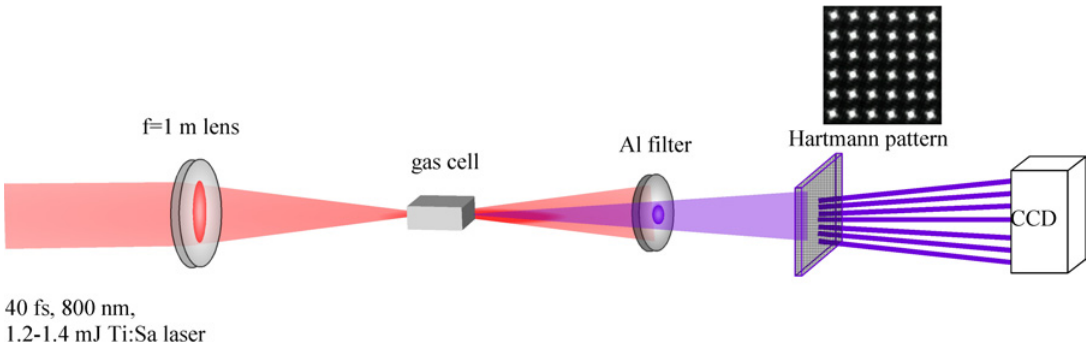

Figure 1. Schematic drawing of the experimental set up showing the diaphragm, the lens, and the gas cell.

2.2. High harmonics wave-front measurement

We present here a study on the HHG wave front evolution versus the generation parameters. The HHG wave front was performed by removing the pinhole in the calibration setup (see fig. 1). Figure 2 presents the absolute measurement of a high harmonic beam generated in an 8 mm length gas cell and for three different gas pressures from 20 to 60 mbar. The best wave front is found being about $0.15\lambda \pm 0.02$ rms (λ/7) on the entire calibrated pupil. Consistent with Lee and collaborators[8], we observe that the wave front is better at the pupil center than at the outer part.

We observed on every measurement that astigmatism was the principle aberration. Since astigmatism is low order aberration and is static, the averaging that may occur during the wave front recording over 1,000 shots might be realistically considered as negligible. This assumption is reinforced by the wave front measurement performed for the IR laser (see fig. 3(a) also exhibiting a strong astigmatism, reproduced identical in every shot. It is realistic to consider that IR laser wave front imprints the HHG wave front. An experiment using an IR deformable mirror, IR Hartmann sensor and a EUV Hartmann sensor confirm the correlation between IR wave-front and HHG wave-front[10]. However, it was surprising to observe that the IR wave-front, having aberrations of about 88 nm rms, generated aberrations for the HHG beam with 4.8 nm rms only. One possibility is that the highly non-linear

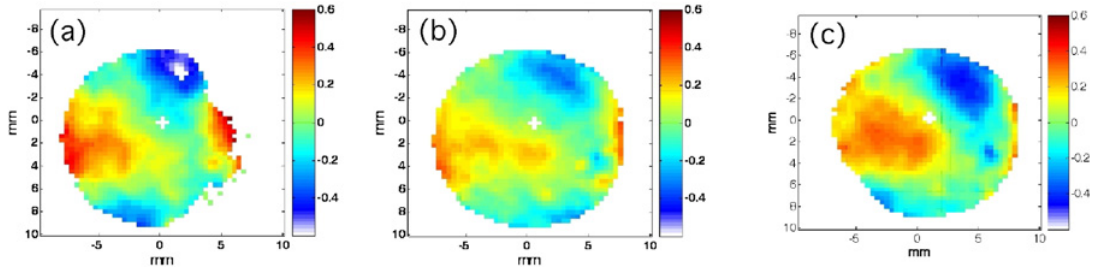

Figure 2. False color maps of the wave fronts measured for an 18 mm diaphragm and for Ar pressure of 25(a), 40(c), 60(e) mbar.

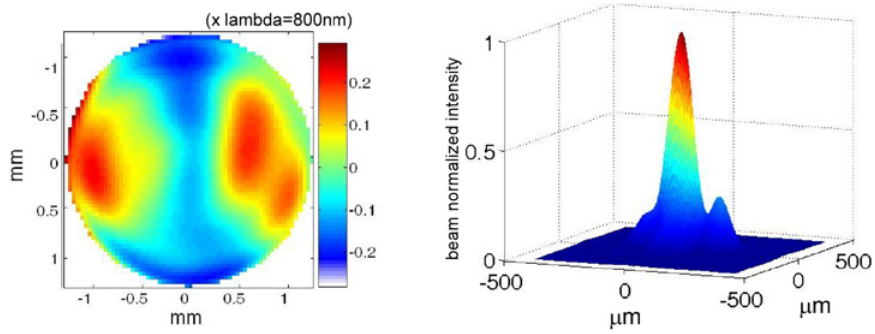

Figure 3. (a) Map in false color of the IR beam wave front recorded on a single shot. The IR beam wave front was very reproducible over the full experiment. (b) IR focal spot calculated by combining both the measured wave front and the intensity maps (not displayed).

process of high harmonics generation prevents high harmonic emission from the most aberrant part of the IR beam because it did not contribute to the main focal spot (fig. 3(b). The low aberration of high harmonics beam allows thigh focalization. This thigh focalization has been used to do damage study and holography experiments.

3. APPLICATIONS OF HIGH HARMONICS LOW ABERRATION WAVE-FRONT

3.1. Damage study

Material removal or laser ablation based on short and ultrashort laser pulse interaction with matter in the infrared, visible and ultra violet (UV) spectral range, has extensively been studied during the past several decades[11, 12]. In the last few decades, a relatively new wavelength regime for laser-induced ablation opened up with the development of the XUV lasers. The various sources provided a large variety of experimental parameters (e.g. pulse duration, pulse energy, peak intensity etc.) for studies of surface modifications and material removal under extreme irradiation conditions. This offered new prospects for the potential use in scientific research (e.g. determination of the damage thresholds of the various elements and compounds, development of optical elements for the transportation and focusing of intense XUV/SXR radiation from the various sources, durability tests) and in industry (e.g. micromachining for the fabrication of diffraction limited microelectronic and micromechanical structures and devices). Two main interaction regimes depending on the laser irradiated fluence have been reported. Subsequently, at low fluences, material damage induced by desorption (desorption or direct photo-etching regime) leading to some physical and chemical surface alterations was observed.

At sufficiently higher fluences, when a certain threshold of the radiation dose was exceeded, material ablation (ablation regime) occurred. In our experiment, we investigated the multi-pulse direct photo-etching by using a high harmonics generation focused on target samples with effective pulse duration less than 10 fs. In achieving this, a polychromatic radiation based on high-order harmonics from the 21^{st} to 27^{th} and with a total energy of $\sim$0.4 nJ per pulse were focused down to a micrometer spot size by a short focal-length parabolic broadband multilayer coating mirror, thus reaching fluences up to 0.3 mJ/cm^2 which is bellow the ablation threshold ($\sim$2 mJ/cm^2). The samples studied were PMMA (poly methyl-methacrylate) deposited on top of silicon substrate. The 3D intensity profile of the XUV beam was reconstructed by means the formed crater profiles on PMMA samples measured by AFM. These profiles are compared to the profile reconstructed by the wavefront sensor placed after the parabola. The focal spot $\sim 1 \times 1\ \mu$m^2 at FWHM retrieved by the calculated PSF is in good agreement with the crater effective diameter.

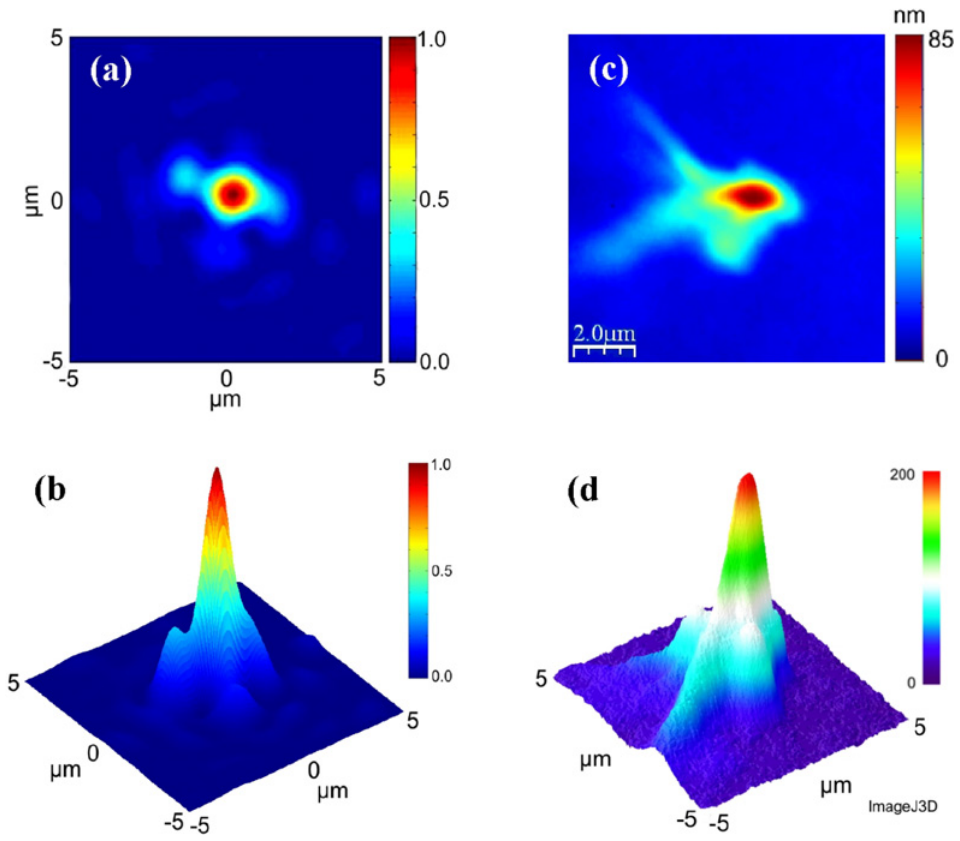

Figure 4. (a) Intensity profile calculated by a point-spread function. (b) The 3D intensity profile. (c) A 2D AFM image of the measured crater profile formed by over 5 s of radiation dose. (d) The reconstructed beam profile after the crater profile in (c).

3.2. Holography experiments

X-UV holography is a promising means for imaging biological and materials science specimens with nanometer-scale resolution. One main advantage of digital holography is that the numerically reconstructed holographic image contains both amplitude and phase information on the object wave.

The advent of sub-femtosecond or even attosecond light pulse will open new fields of time-resolved studies with unprecedented resolution. Using attosecond pulses as a source for digital holography will enable us to reach amplitude and phase microscopy with high temporal and spatial resolution. D. Gabor invented holography in 1948 as a method for recording and reconstructing amplitude and phase of a wave field[13]. A hologram is the photographically or otherwise recorded interference pattern between a wave field scattered from the object and a coherent background named reference wave. It is usually recorded on a flat surface, but contains the information about the entire three-dimensional wave field. The first soft x-ray hologram with a high harmonics source was made by Bartels and collaborators in 2002[4]. They obtained a resolution of 8 μm. The advantages of this source are to be tabletop and intrinsically spatially coherent. In this experience we use digital in-line holography Microscopy (DIHM). The term Digital means that the recording of the hologram is made by a Charged Coupled Devices (CCD) and the reconstruction is numerical. This method enables now full digital recording and processing of holograms, without any photographic recording as an intermediate step. Direct recording and numerical reconstruction have the potential to permit real-time observation. Microscopy is used to reduce the resolution of the detector[14]. By introducing a magnification factor (M), the resolution of the used CCD is reduced from 13.5 μm to 13.5 μm/M. If the magnification is high enough the resolution, Res, is only limited by the numerical aperture, NA, defined by the optical system: Res $= 0.61 \times \lambda$/NA. The experimental setup is presented in fig. 5. Soft X-ray radiation (H29 $\lambda = 27.6$ nm; H27 $\lambda = 29.6$ nm; H25 $\lambda = 32$ nm; H23 $\lambda = 34.8$ nm) is generated by focusing a Ti:sapphire laser in a gas cell filled with argon. On B_4C/Si multilayer is used to select the 25th Harmonic. The soft x-ray radiation is then focused with a 2.5° off axis parabola near the sample. The sample is a microscope fiber tip with an apex radius varying continuously from 4 μm to 50 nm.

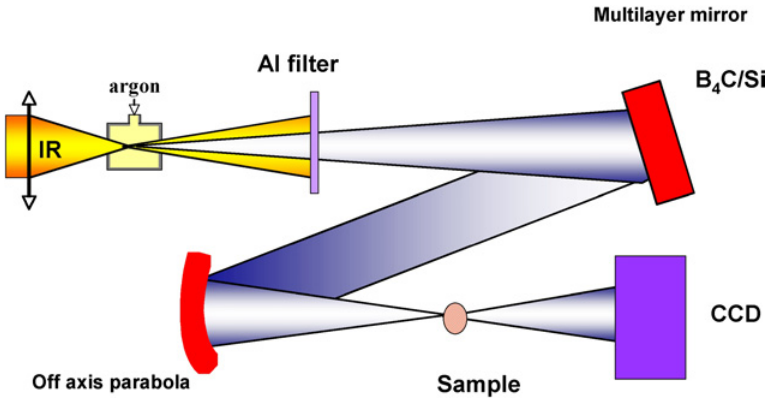

Figure 5. Schematic drawing of the soft-x-ray holographic setup.

The contrast image (hologram), obtained by subtracting the images with and whithout the object, is presented in fig. 6(a). Hologram have been recorded with 1000 shots of roughly 10^8 photon/pulse/harmonic. The general principle of digital reconstruction consists of backdiffracting the hologram by the reference wave. It can be described by the Fresnel-Kirchhoff integral. The holographic reconstruction is presented in fig. 6(b). We estimate the NA to be about 0.037, giving a theoretical spatial resolution of 520 nm. The experimental resolution measured as the full width at half-maximum of the wire is 610 nm.

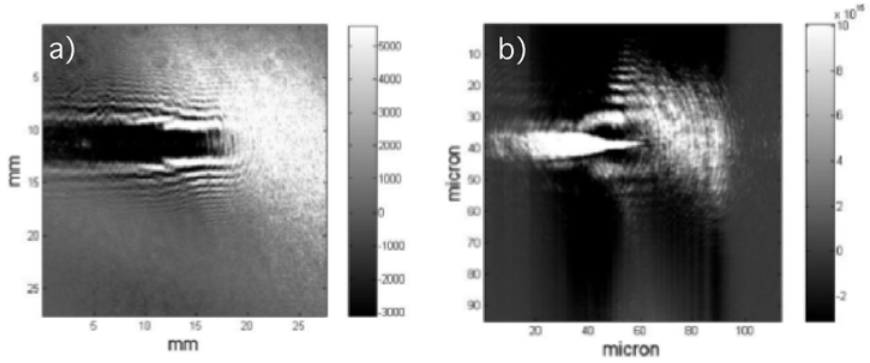

Figure 6. Hologram and reconstruction.

4. CONCLUSIONS

This works demonstrates the capability to use high harmonics generation sources for applications. Indeed the high quality wave-front allows tight focusing experiments. Multiple-pulse material desorption has been observed in PMMA by tightly focusing high-order harmonics with an effective photon energy at 39 eV and a bandwidth at FWHM 15 eV down to a micrometer spot size. Holograms of thin wires were also recorded. Resolution of 610 nm has been attained. To achieve even better resolution, a NA of around 0.5 is necessary. The harmonic photon flux should be also improved at least by a factor of 10 to have access to single-shot, femtosecond experiments. Promising techniques using, for example phase matching improving[15] or multi-color fields[16] can be implemented to reach this aim.

Acknowledgement

This work has been supported by the TUIXS- FP6 NEST-Adventure n. 012843. Multilayer depositions have been carried on the CEMOX's machine implemented by PraXO.

References

[1] W. Chao et al., Nature. **435**, (2005) 1210.
[2] J.Filevich et al.,Appl. Opt **43**, (2004) 3398.
[3] A.S. Morlens et al.,Apt. Lett . **31**, (2006) 3095-3097
[4] R.A. Bartels et al..,Science **297**, (2002) 376
[5] H.T Kim et al.,Appl. Phys B **78**, (2004) 863
[6] L.Le Derroff et al.,Phys. Rev. A**61**, (2000) 043802
[7] J.W. Goodman, *Introduction to Fourier optics* (Robert and Company,Englewood 2005) 491
[8] D.G Lee et al.,Opt. Lett.**28**, (2003) 480-482
[9] P. Mercere et al.,Opt. Lett.**28**, (2003) 1534
[10] C.Valentin et al.,J.Opt.Soc Am. B **25**, (2008) 761
[11] P.E. Dyer, Appl. Phys. Lett. A**77**,(2003)167
[12] E.G. Gamaly et al.,Phys. of Plasm.**9**, (2003) 949.
[13] D.Gabor,Nature**161**, (1948) 777
[14] J.Garcia-Sucerquia et al.,Appl. Opt.**45**, (2005) 836
[15] R.Bartels et al.,Nature.**406**, (2000) 164
[16] I.J.Kim et al.,Phys. Rev. Lett. **94**, (2005) 243901